Journal of The Electrochemical Society, **152** (9) C620-C625 (2005)
0013-4651/2005/152(9)/C620/6/$7.00 © The Electrochemical Society, Inc.

Electrodeposition of Al-Mo-Mn Ternary Alloys from the Lewis Acidic $AlCl_3$-EtMeImCl Molten Salt

Tetsuya Tsuda,[a,*] Charles L. Hussey,[a,,z] and Gery R. Stafford[b,*]**

[a]*Department of Chemistry and Biochemistry, The University of Mississippi, University, Mississippi 38677, USA*
[b]*Materials Science and Engineering Laboratory, National Institute of Standards and Technology, Gaithersburg, Maryland 20899, USA*

The electrodeposition of Al-Mo-Mn ternary alloys was examined in the Lewis acidic 66.7-33.3% mole fraction (mol %) aluminum chloride-1-ethyl-3-methylimidazolium chloride ($AlCl_3$-EtMeImCl) molten salt containing Mo(II) and Mn(II). By adjusting the $C_{Mn(II)}/C_{Mo(II)}$ concentration ratio in the plating solution and employing different current densities, it was possible to prepare alloys with widely varying compositions and surface morphologies. All Al-Mo-Mn alloys were dense, compact, and adhered well to the copper substrate surface. The addition of small amounts of Mn to the Al-Mo alloy resulted in an improvement in the chloride pitting corrosion resistance and metallic brightness. For example, $Al_{90.1}Mo_{9.9}Mn_0$ and $Al_{89.5}Mo_{9.1}Mn_{1.4}$ displayed pitting potentials that were 725 and 837 mV more positive than that for Al, respectively. Al-Mo-Mn alloys that contained more than about 10 atom % Mo + Mn exhibited a metallic glass structure.
 [DOI: 10.1149/1.1995696]

Manuscript submitted January 28, 2005; revised manuscript received April 8, 2005. Available electronically July 28, 2005.

The electrodeposition of Al-transition metal alloys from the Lewis acidic room-temperature chloroaluminate molten salt, aluminum chloride-1-ethyl-3-methylimidazolium chloride ($AlCl_3$ - EtMeImCl), has been investigated as an alternative to conventional nonequilibrium methods for preparing these corrosion-resistant alloys. Among the alloys that have been electrodeposited from this or related chloroaluminate melts are Al-Ti,[1-3] Al-Zr,[4,5] Al-Hf,[5] Al-V,[6] Al-Cr,[7-9] Al-Ni,[10-12] Al-Co,[13-16] and Al-Cu.[17-20] Progress in this area has been reviewed.[21] More recently, we reported a method for plating Al-Mo alloys from the 66.7–33.3% mole fraction (mol %) composition of this molten salt containing dissolved $(Mo_6Cl_8)Cl_4$.[22] The resulting electrodeposited Al-Mo alloys showed better resistance to chloride-induced pitting corrosion than any of the alloys listed above, and they exhibited a metallic brightness suitable for surface finishing. Amorphous Al-Mn alloys produced from inorganic chloroaluminate molten salts containing dissolved $MnCl_2$ are also reported to exhibit good metallic brightness and improved resistance to chloride pitting corrosion compared to pure Al.[23-26] Although it is possible that the addition of Mn to Al-Mo alloys may result in a ternary alloy with properties superior to those of the parent binary alloys, Al-Mo and Al-Mn, respectively, there is a paucity of reports describing such investigations. In this article, we report the results of a preliminary investigation of the electrodeposition of Al-Mo-Mn alloys that was undertaken in the 66.7–33.3 mol % $AlCl_3$ -EtMeImCl molten salt.

Experimental[c]

Preparation of the plating bath.— The procedures used for the synthesis of EtMeImCl, the purification of $AlCl_3$ by sublimation, and the preparation and purification of a Lewis acidic 66.7–33.3 mol % $AlCl_3$-EtMeImCl molten salt were identical to those described in previous articles.[6,27] Anhydrous manganese(II) chloride, $MnCl_2$ (Aldrich, 99.99%), and anhydrous molybdenum(II) chloride, $(Mo_6Cl_8)Cl_4$ (Cerac, 99.5%), were used as received and were dissolved directly in the $AlCl_3$-EtMeImCl molten salt to prepare plating baths. After preparing the solutions of Mo(II) and Mn(II) individually, the plating bath for electrodeposition of the Al-Mo-Mn ternary alloys was adjusted by combining the solutions as needed. All experiments were carried out in a nitrogen gas-filled glove box (Vacuum Atmospheres Co., NEXUS system) with an O_2 and H_2O content <3 ppm.

Electrochemical experiments.— Electrochemical experiments were conducted with an EG&G PARC model 263A potentiostat/galvanostat. This instrument was controlled with a desktop computer utilizing EG&G PARC model 270 software. The electrodeposition of the ternary aluminum alloys described below was performed with an EG&G PARC model 173 potentiostat/galvanostat equipped with a model 179 digital coulometer plug-in module. All electrochemical experiments were carried out in three-electrode cells. Electronic resistance compensation was employed during voltammetric experiments. A Pine Instruments Teflon-sheathed Pt disk electrode with a geometrical area of 0.099 cm^2 or a glassy carbon disk electrode with a geometrical area of 0.247 cm^2 was employed as the working electrode for voltammetry experiments. Coils of 0.10 cm diam Al wire (Alfa Aesar, 99.999%) were used for the counter and reference electrodes. These electrodes were immersed in melt with the same composition as the bulk melt, but were separated from the bulk melt by a porosity E glass frit (Ace Glass). The Al electrodes were cleaned with a mixture of concentrated H_2SO_4, HNO_3, and H_3PO_4, rinsed with distilled water, and dried under vacuum before use. Alloy samples of approximately 10 μm thickness were deposited from solutions of Mo(II), Mn(II), or Mo(II) + Mn(II) onto working electrodes consisting of a length of 1.25 mm diam Cu wire. The substrates were rotated at a fixed rate of 209 rad s^{-1} with a Pine Instruments AFMSRX electrode rotator as described in previous reports.[1,7,22] At the conclusion of each deposition experiment, the alloy-plated substrate was removed from the glove box and cleaned with distilled water.

Potentiodynamic pitting measurements were carried out on these alloy samples at room temperature in a 0.1 mol L^{-1} solution of NaCl in distilled water. This solution was deaerated with nitrogen gas for several hours before each experiment. The reference electrode for these measurements was a sodium-saturated calomel electrode (SSCE), and the counter electrode was a large surface area Pt wire coil. A known length of the plated Cu wire was exposed to the NaCl solution by using a heat-shrink tubing mask, and the sample was scanned at 0.5 mV s^{-1} by using linear staircase voltammetry.

Characterization of the electrodeposits.— The crystal structures of the electrodeposits were examined with standard X-ray diffraction (XRD) techniques by using a Siemens D-500 X-ray diffractometer at the National Institute of Standards and Technology (NIST). This instrument was operated in the θ-2θ scan mode and employed Cu Kα radiation. Surface morphology and elemental analysis of the

* Electrochemical Society Active Member.
** Electrochemical Society Fellow.
z E-mail: chclh@chem1.olemiss.edu

[c]NOTE: Certain trade names are mentioned for experimental information only; in no case does it imply a recommendation or endorsement by NIST.

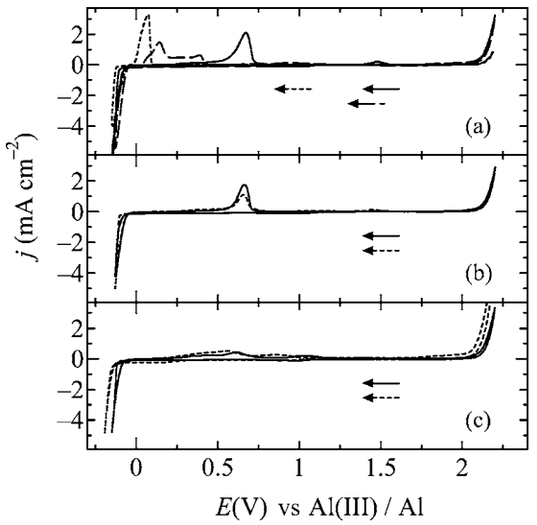

Figure 1. Cyclic voltammograms recorded at a stationary Pt disk electrode in the 66.7–33.3 mol % $AlCl_3$-EtMeImCl melt: (a) (---) pure melt, (—) 35.5 mmol L^{-1} Mo(II), (– – –) 35.5 mmol L^{-1} Mn(II); (b) (—) 35.5 mmol L^{-1} Mo(II) + 17.8 mmol L^{-1} MN(II), (---) 35.5 mmol L^{-1} Mo(II) + 35.5 mmol L^{-1} Mn(II); and (c) (—) 35.5 mmol L^{-1} Mo(II) + 71.0 mmol L^{-1} Mn(II), (---) 35.5 mmol L^{-1} Mo(II) + 143 mmol L^{-1} Mn(II). The temperature was 32.8 K, and the scan rate was 10 mV s^{-1}.

alloy samples were performed with a JEOL JSM-6100 (The University of Mississippi) or a JEOL JXA-840 (NIST) scanning electron microscope (SEM). Alloy composition was measured with energy-dispersive X-ray spectroscopy (EDS) on the as-deposited surfaces with pure Al, Mo, and Mn as standards. The chlorine content of the alloys, which reflects contamination by chloride from the plating bath, was also estimated with EDS. The detection limit for chlorine was ~0.1 atom %.

Results and Discussion

Cyclic staircase voltammetry.— $(Mo_6Cl_8)Cl_4$ and $MnCl_2$ were dissolved readily in the Lewis acidic 66.7–33.3 mol % $AlCl_3$ -EtMeImCl molten salt to produce yellow and transparent solutions, respectively. Figure 1a shows cyclic staircase voltammograms recorded at a Pt stationary disk electrode in the pure 66.7–33.3 mol % melt and after the dissolution of these compounds. To record these voltammograms, the potential scan was initiated from the rest potential to a potential sufficiently cathodic to electrodeposit aluminum. The scan was then reversed until it reached the positive limit of the melt at +2.2 V and was finally returned to the initial potential. The negative and positive potential limits of the Lewis acidic $AlCl_3$-EtMeImCl molten salt arise from the reduction of the coordinately unsaturated $Al_2Cl_7^-$ ion to Al metal and the oxidation of the $AlCl_4^-$ ion to chlorine gas, respectively[21]

$$4Al_2Cl_7^- + 3e^- \rightleftharpoons Al + 7AlCl_4^- \quad [1]$$

$$2AlCl_4^- \rightleftharpoons Al_2Cl_7^- + 1/2Cl_2 + e^- \quad [2]$$

As is typically observed during the electrodeposition of Al on Pt in the pure melt, a small nucleation overpotential was required to initiate the Al deposition process. Voltammograms recorded in solutions containing Mo(II) or Mn(II) are also shown in Fig. 1a. These voltammograms are identical to those reported previously.[22,28] The cathodic portions of these voltammograms show essentially the same features as voltammograms that were acquired in pure melt. That is, there are no obvious reduction waves associated with Mo(II) or Mn(II), signifying that neither species undergoes reduction before Al deposition commences. However, the anodic portions of these voltammograms exhibit stripping waves that are associated with the oxidation of electrodeposited Al-Mo and Al-Mn alloys.

The voltammograms that were recorded in solutions containing both Mo(II) and Mn(II) (Fig. 1b and c) were sensitive to the Mn(II)/Mo(II) concentration ratio, $C_{Mn(II)}/C_{Mo(II)}$. When $C_{Mn(II)}/C_{Mo(II)} \leqslant 1$ (Fig. 1b), the appearance of the voltammogram is similar to that recorded in the melt containing only Mo(II). However, the deposition potential for Al shifts to slightly more negative potentials, and the current for the stripping wave at ~0.6 V becomes smaller as the Mn(II) concentration is increased. The overpotential for Al deposition eventually exceeds 0.13 V when $C_{Mn(II)}/C_{Mo(II)} = 4$ (Fig. 1c), and the current for the stripping wave at ~0.6 V nearly disappears. These results imply that the Al-Mo-Mn electrodeposition process varies with $C_{Mn(II)}/C_{Mo(II)}$ and that the addition of Mn(II) to the plating solution inhibits the nucleation of Al. Similar results were found when Mn(II) was added to the $AlCl_3$-NaCl melt.[26,29] The electrodeposition of Al-Mo-Mn alloys was investigated further by preparing bulk alloy deposits using controlled-current techniques as discussed below.

Electrodeposition of Al-Mo-Mn alloys.— Controlled-current techniques were employed to prepare Al-Mo-Mn alloy samples for detailed compositional and morphological analysis. To simplify the discussions below, the total applied current density is designated as j_t. An increase in the value of $-j_t$ signifies an increase in the heterogeneous reaction rate of the cathodic electrode reaction per unit electrode area. All bulk electrodeposition experiments were conducted at copper rotating wire electrodes (Cu-RWE) at a rotation rate of 209 rad s^{-1} using the same procedures described in previous articles.[1,7,22] The deposition conditions that were used during these experiments and the alloys that resulted are described in Table I. The data in this table reveal that the transition metal content of the electrodeposited Al-Mo-Mn alloys, i.e., the combined atomic percent fraction of Mo + Mn, varies with j_t, $C_{Mo(II)}$, and $C_{Mn(II)}$. This behavior is illustrated graphically in Fig. 2. When $C_{Mn(II)}/C_{Mo(II)} \leqslant 1$, the Mo + Mn content decreased with an increase in $-j_t$. However, the Mo + Mn content was more or less independent of the current density when $C_{Mn(II)}/C_{Mo(II)} = 2$, exhibiting only a shallow minimum between 5 and 40 mA cm^{-2}. If $C_{Mn(II)}/C_{Mo(II)} = 4$, then a similar minimum was observed at small values of $-j_t$, but as $-j_t$ was increased above ~20 mA cm^{-2}, the Mo + Mn content increased.

In order to better understand the dependence of the Mo + Mn content of the alloy on the plating variables, the amounts of Mo and Mn in the plated Al-Mo-Mn alloys were plotted individually in Fig. 3 as a function of current density. This figure reveals several important trends. First, as shown in the upper panel, the Mo content of the alloy always decreases with an increase in $-j_t$, regardless of $C_{Mo(II)}$, $C_{Mn(II)}$, or $C_{Mn(II)}/C_{Mo(II)}$. Second, at a fixed value of $-j_t$ and constant $C_{Mo(II)}$, the addition of Mn(II) to the plating solution suppresses the amount of Mo in the alloy deposit; this effect becomes more pronounced as $C_{Mn(II)}$ is increased. Third, the data in the lower panel of Fig. 3 indicate that there is no significant reciprocal effect, i.e., the addition of Mo(II) to a plating solution with a fixed $C_{Mn(II)}$ has little or no effect on the amount of Mn incorporated into the electrodeposit during the deposition reaction. Fourth, the data in the lower panel of Fig. 3 indicate that when $C_{Mn(II)}$ is increased beyond 35.5 mmol L^{-1}, the Mn content of the alloy increases with an increase in $-j_t$. This phenomenon is most pronounced when $C_{Mn(II)}$ = 143 mmol L^{-1} or $C_{Mn(II)}/C_{Mo(II)} = 4$.

The composition data in Fig. 3 were converted to partial current densities by using the following expressions

$$j_{Mo} = 2j_t x_{Mo}/(3 - x_{Mo} - x_{Mn}) = 2j_t x_{Mo}/(2 + x_{Al}) \quad [3]$$

$$j_{Mn} = 2j_t x_{Mn}/(3 - x_{Mo} - x_{Mn}) = 2j_t x_{Mn}/(2 + x_{Al}) \quad [4]$$

Table I. Summary of electrodeposited Al-Mo-Mn alloys.[a]

Deposition conditions			Alloy properties		
Current density (mA cm^{-2})	$C_{Mo(II)}$ (mmol L^{-1})	$C_{Mn(II)}$ (mmol L^{-1})	Mo content (atom %)	Mn content (atom %)	Pitting potential (mV vs SSCE)
ca. −10 to −40	0	0	0	0	−683
−30	35.5	0	7.3	0	13
−20	35.5	0	8.1	0	131
−15	35.5	0	8.9	0	111
−10	35.5	0	9.9	0	42
− 5	35.5	0	10.7	0	—
−80	0	35.5	0	3.6	—
−40	0	35.5	0	5.7	−317
−20	0	35.5	0	4.2	−368
−10	0	35.5	0	2.6	−439
− 5	0	35.5	0	3.0	−407
−80	35.5	17.8	2.1	2.1	—
−40	35.5	17.8	4.4	2.8	—
−20	35.5	17.8	6.2	2.1	71
−10	35.5	17.8	9.1	1.4	154
− 5	35.5	17.8	10.0	1.2	185
−80	35.5	35.5	1.8	3.1	—
−40	35.5	35.5	2.2	5.4	—
−20	35.5	35.5	5.8	3.0	—
−10	35.5	35.5	8.0	2.3	—
− 5	35.5	35.5	10.1	1.2	—
−80	35.5	71.0	1.1	8.7	—
−40	35.5	71.0	2.6	7.6	—
−20	35.5	71.0	2.5	6.5	178
−10	35.5	71.0	5.5	3.7	11
− 5	35.5	71.0	7.8	2.5	—
−80	35.5	143	1.0	16.7	−110
−40	35.5	143	1.6	13.2	−44
−20	35.5	143	4.0	7.6	65
−10	35.5	143	4.9	6.3	122
− 5	35.5	143	7.6	4.5	97

[a] Alloys were electrodeposited at 328 K from a 66.7 mol % $AlCl_3$-EtMeImCl plating bath on a copper wire substrate rotated at 209 rad s^{-1}.

$$j_{Al} = j_t - j_{Mo} - j_{Mn} \quad [5]$$

where $-j_{Mo}$, $-j_{Mn}$, and $-j_{Al}$ represent the average partial current densities for Mo, Mn, and Al deposition, respectively, during the deposition process, and x_{Mo}, x_{Mn}, and x_{Al} are the atomic fractions of Mo, Mn, and Al, respectively, in the electrodeposited Al-Mo-Mn alloys listed in Table I. Plots of $-j_{Mo}$, $-j_{Mn}$, and $-j_{Al}$ vs $-j_t$ are given in Fig. 4. These plots provide insight into the observed dependence of the combined (Fig. 2) and individual (Fig. 3) Mo and Mn content of the alloys on the current density.

Figure 4 shows that for all purposes $-j_{Al}$ is a linear function of $-j_t$. $-j_{Mo}$ reaches a limiting value when $-j_t \geq 20$ mA cm^{-2}. Furthermore, the limiting value of $-j_{Mo}$ decreases when $C_{Mn(II)}$ is increased; that is, Mn(II) inhibits the deposition of Mo. Thus, in all cases, $-j_{Mo}$ becomes a smaller fraction of the total current density as $-j_t$ is increased. This explains why the Mo content of the Al-Mo-Mn alloy always decreases with an increase $-j_t$, as indicated in the upper panel of Fig. 3. Taken together with the voltammetric results presented above, these results indicate that the Mo deposition potential must be approximately the same or perhaps slightly negative of the Al deposition potential. Because the Mo(II) concentration in the plating solution was always much smaller than the concentration of the reducible Al(III) species, $Al_2Cl_7^-$ (35.5 mmol L^{-1} vs 3.29×10^3 mmol L^{-1}, respectively), the limiting value for $-j_{Mo}$ is attained at relatively small values of $-j_t$. The decrease in the Mo content of the Al-Mo-Mn alloy with increasing $-j_t$ described above is identical to that found during a previous investigation of the electrodeposition of binary Al-Mo alloys from solutions of Mo(II) in the 66.7 mol % $AlCl_3$-EtMeImCl melt.[22]

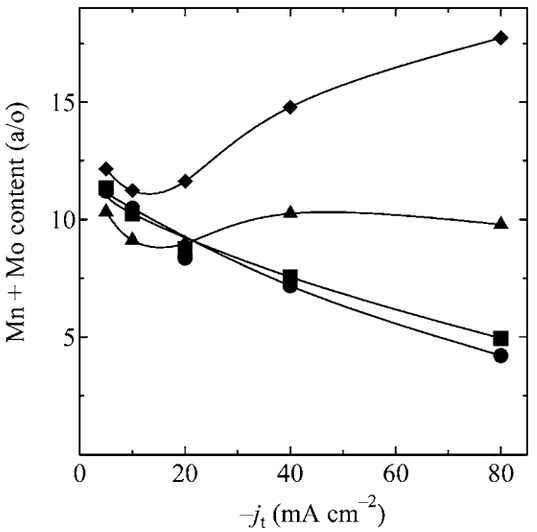

Figure 2. Relationship between the plating current density, the atomic percent fraction of Mo + Mn in the Al-Mo-Mn alloy, and the composition of the plating solution: (●) 35.5 mmol L^{-1} Mo(II) + 17.8 mmol L^{-1} Mn(II); (■) 35.5 mmol L^{-1} Mo(II) + 35.5 mmol L^{-1} Mn(II); (▲) 35.5 mmol L^{-1} Mo(II) + 71.0 mmol L^{-1} Mn(II); (♦) 35.5 mmol L^{-1} Mo(II) + 143 mmol L^{-1} Mn(II). The temperature was 328 K, and the substrate was rotated at 209 rad s^{-1} during deposition.

The plots of $-j_{Mn}$ vs $-j_t$ shown in Fig. 4 display considerably different behavior than the plots of $-j_{Mo}$ vs $-j_t$. The primary difference is that $-j_{Mn}$ increases with $-j_t$; this behavior is most obvious when $C_{Mn(II)} \geq 71.0$ mmol L^{-1}. The electrodeposition of binary

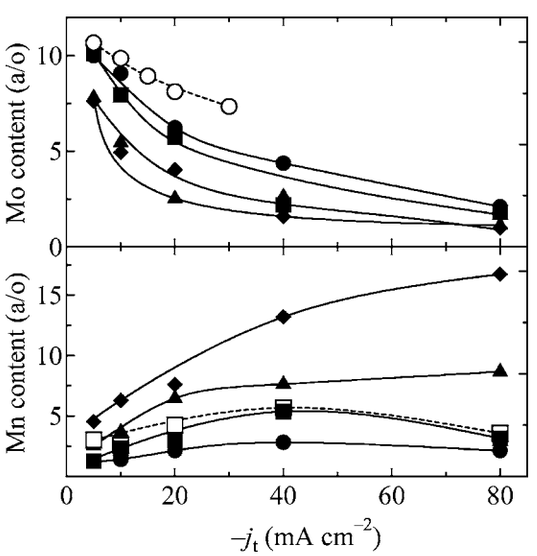

Figure 3. Relationship between the plating current density, the atomic precent fraction of Mo (upper panel) and Mn (lower panel), and the plating solution composition: (○) 35.5 mmol L^{-1} Mo(II), (□) 35.5 mmol L^{-1} Mn(II); (●) 35.5 mmol L^{-1} Mo(II) + 17.8 mmol L^{-1} Mn(II); (■) 35.5 mmol L^{-1} Mo(II) + 35.5 mmol L^{-1} Mn(II); (▲) 35.5 mmol L^{-1} Mo(II) + 71.0 mmol L^{-1} Mn(II); (♦) 35.5 mmol L^{-1} Mo(II) + 143 mmol L^{-1} Mn(II).

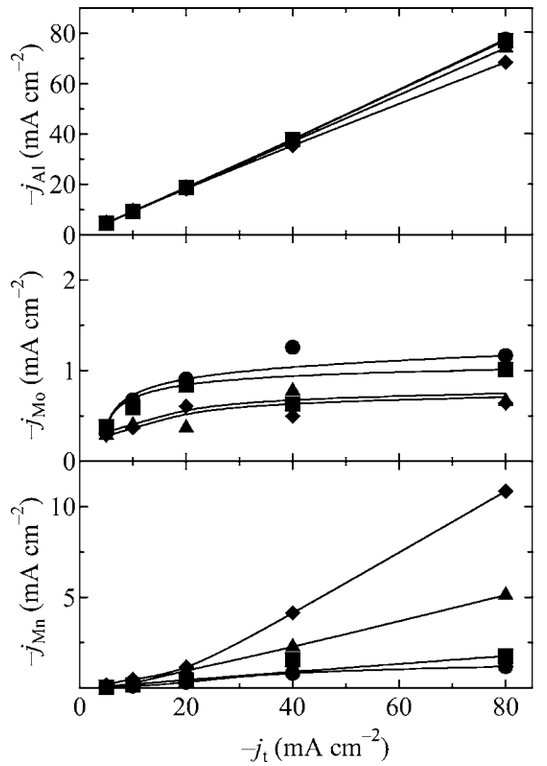

Figure 4. Plots of the partial current densities for the deposition of Al (upper panel), Mo (middle panel), and Mn (lower panel) vs the total current density. The solution compositions were: (●) 35.5 mmol L^{-1} Mo(II) + 17.8 mmol L^{-1} Mn(II); (■) 35.5 mmol L^{-1} Mo(II) + 35.5 mmol L^{-1} Mn(II); (▲) 35.5 mmol L^{-1} Mo(II) + 71.0 mmol L^{-1} Mn(II); (♦) 35.5 mmol L^{-1} Mo(II) + 143 mmol L^{-1} Mn(II).

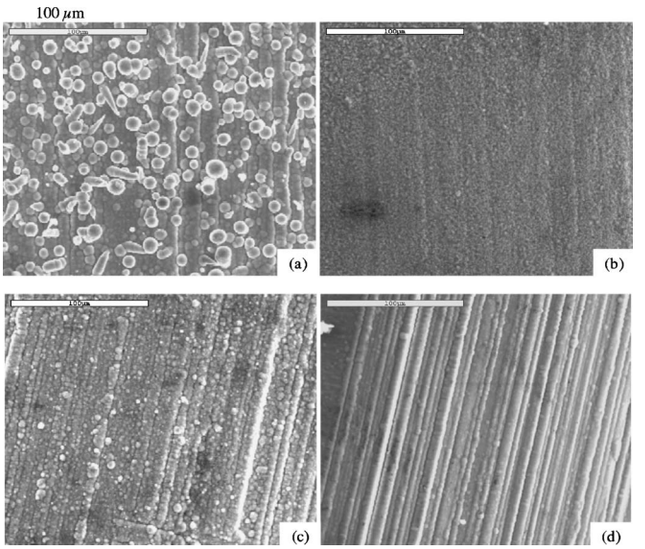

Figure 5. SEM images of electrodeposited Al-Mo-Mn alloy samples. The alloy compositions, current densities, and solution compositions were: (a) $Al_{89.7}Mo_{8.0}Mn_{2.3}$, −10 mA cm^{-2}, 35.5 mmol L^{-1} Mo(II) + 35.5 mmol L^{-1} Mn(II); (b) $Al_{92.4}Mo_{2.2}Mn_{5.4}$, −40 mA cm^{-2}, 35.5 mmol L^{-1} Mo(II) + 35.5 mmol L^{-1} Mn(II); (c) $Al_{88.8}Mo_{4.9}Mn_{6.3}$, −10 mA cm^{-2}, 35.5 mmol L^{-1} Mo(II) + 143 mmol L^{-1} Mn(II), and (d) $Al_{85.2}Mo_{1.6}Mn_{13.2}$, −40 mA cm^{-2}, 35.5 mmol L^{-1} Mo(II) + 143 mmol L^{-1} Mn(II).

Al-Mn alloys has been studied extensively in the Lewis acidic $AlCl_3$-NaCl melt.[21] Of these previous investigations, the most systematic study was carried out by Stafford,[26] who examined the electrodeposition of Al-Mn from solutions of $MnCl_2$ in the 66.7 mol % $AlCl_3$-NaCl melt under controlled-potential conditions. In this investigation, the Mn deposition potential was found to be negative of that for Al deposition, i.e., Al is more noble than Mn. Although these findings were derived from controlled-potential experiments, they nevertheless provide the basis for a qualitative explanation of the dependence of the Mn content of the alloy on $C_{Mn(II)}$ and $-j_t$ found during the present investigation. For example, if the Mn deposition potential is negative of that for Al in the 66.7 mol % $AlCl_3$ - EtMeImCl melt, then the application of a small cathodic current would produce deposits that are rich in Al. However, the Mn content of the alloys should increase as $-j_t$ is increased, because increasing $-j_t$ is increased, because increasing $-j_t$ drives the electrode potential to more negative values and accelerates the Mn deposition reaction.

The analysis of the partial current densities presented above provides a qualitative explanation for the general result that Al-Mo-Mn alloys rich in Mo are obtained at small values of $-j_t$, whereas alloys rich in Mn are obtained at large values of $-j_t$, provided that $C_{Mn(II)}/C_{Mo(II)} \geq 2$. This analysis also reveals that the codeposition of Al, Mo, and Mn displays classical anomalous behavior. That is, the addition of Mn(II) to the plating solution suppresses the partial current for the codeposition of the more noble transition metal component, Mo, thereby enhancing the amount of the less noble component, Mn, in the resulting electrodeposit. As expected, experiments conducted with melt solutions originally containing only Mn(II) show that the addition of Mo(II) to these plating solutions does not affect $-j_{Mn}$.

Characterization of the electrodeposited Al-Mo-Mn alloys.— Figure 5 shows SEM images of typical "as-deposited" bulk Al-Mo-Mn alloy samples that were prepared under different deposition conditions. In every case, these alloy samples appeared to nucleate along the striations of the drawn copper wire substrate. The deposition charge used to prepare these samples was, in theory, sufficient to produce an atomically smooth layer of pure Al that was ~10 μm in thickness. All of the alloy deposits prepared during this investigation were found to be chloride-free. Figures 5a and b illustrate the surface morphology of ternary alloys produced at different current densities under the condition that $C_{Mn(II)}/C_{Mo(II)} = 1$. As discussed in the previous section, the current density controls not only the Al/(Mo + Mn) ratio in the alloy, but also the Mo/Mn ratio. The deposit shown in Fig. 5a was prepared at a relatively low current density (−10 mA cm^{-2}) and contains 8.0 atom % Mo and 2.3 atom % Mn. The surface of this deposit consists of spherical or cone-shaped nodules that are 5–15 μm in diameter. However, the deposit prepared at a higher current density (−40 mA cm^{-2}) in the same plating solution (Fig. 5b) contains less Mo (2.2 atom %) and more Mn (5.4 atom %) than the deposit in Fig. 5a. The surface morphology of this deposit consists of very small, densely packed crystallites. If $C_{Mn(II)}/C_{Mo(II)} \approx 4$, then the deposit prepared at −10 mA cm^{-2} contains 4.9 atom % Mo and 6.3 atom % Mn and consists of random spherical nodules that are 5–10 μm in diameter (Fig. 5c). At −40 mA cm^{-2}, the deposit prepared in this same solution contains 1.6 atom % Mo and 13.2 atom % Mn (Fig. 5d). Visually, this deposit presents a nearly specular surface.

XRD analysis of the as-deposited samples revealed that those electrodeposits containing less than approximately 10 atom % Mo + Mn exhibited two phases. The diffraction pattern for these deposits consisted of the typical reflections for face-centered cubic (fcc) Al and a broad reflection due to an amorphous phase (Fig. 6). When the combined amounts of Mo and Mn exceeded 10 atom %, only a single broad reflection centered at $2\theta = 41°$ was observed in the diffraction pattern, suggesting that the deposit was completely amorphous. This result was very similar to that found during the electrodeposition of amorphous Al-Mo.[22] That is, the crystal structures of the Al-Mo-Mn deposits are very dependent on the amount of the

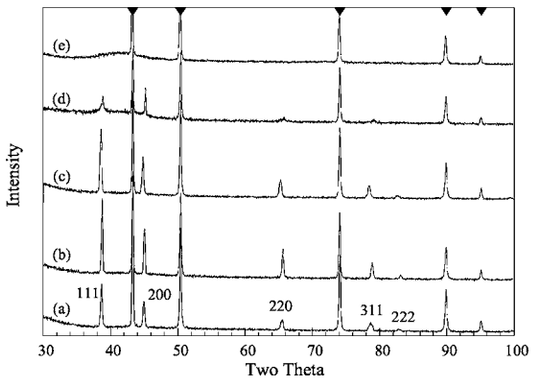

Figure 6. XRD patterns (Cu K α) from as-deposited alloys: (a) $Al_{95.8}Mo_{2.1}Mn_{2.1}$, (b) $Al_{92.8}Mo_{4.4}Mn_{2.8}$, (c) $Al_{92.4}Mo_{2.2}Mn_{5.4}$, (d) $Al_{89.8}Mo_{2.6}Mn_{7.6}$, and (e) $Al_{89.7}Mo_{7.8}Mn_{2.5}$. Copper reflections from substrate denoted by (▼) at the top of the figure (*JCPDS card no. 4-0836, Powder Diffraction File*. 1996, International Center for Diffraction Data, Newtown Square, PA.).

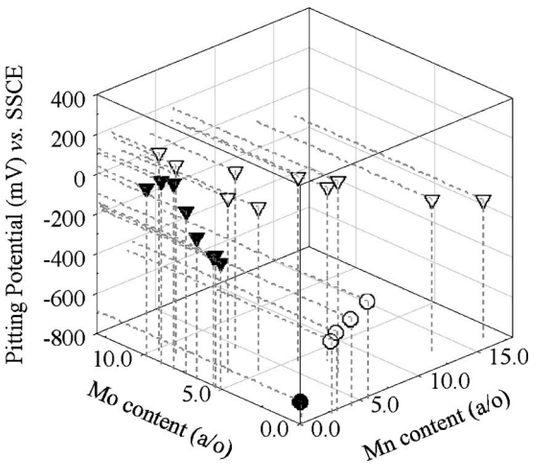

Figure 8. Pitting potentials of electrodeposited Al-Mn-Mo alloys: (●) pure Al, (○) Al-Mn, (▼) Al-Mo, and (▽) Al-Mo-Mn.

transition metal in the Al alloy deposit, and when this concentration exceeds a certain threshold, a metallic glass phase begins to develop in the electrodeposit. However, in the present case, the formation of a glass phase depends on the combined amounts of both Mo and Mn in the alloy.

Pitting potential measurements.— The pitting potentials of the electrodeposited Al-Mo-Mn alloys were determined by carrying out potentiodynamic anodic polarization experiments in deaerated aqueous NaCl with the samples described above. Some examples of the resulting potentiodynamic current-potential curves are shown in Fig. 7. As noted for the individual alloys, i.e., Al-Mo[22] and Al-Mn,[23] the Al-Mo-Mn alloys are spontaneously passive at the rest potential of the solution. During anodic polarization, they display a stable passive region characterized by a small, potential-independent current followed by an abrupt rise in current at the pitting potential. The variation of the pitting potential with alloy composition is given in Table I and Fig. 8. This figure shows that the addition of relatively modest amounts of Mo and Mn to the alloy results in a significant increase in the pitting potential compared to pure Al. Furthermore, the addition of both Mo and Mn to the alloy results in deposits with greater resistance to pitting corrosion than a comparable binary alloy containing only one of these transition metal components. For example, Table I and Fig. 8 show that the pitting potential of an Al-Mo-Mn alloy containing approximately 10 atom % (Mo + Mn), e.g., $Al_{89.5}Mo_{9.1}Mn_{1.4}$, is more positive than that for Al-Mo containing about 10 atom % Mo, e.g., $Al_{90.1}Mo_{9.9}Mn_0$. Thus, the pitting corrosion resistance of Al is substantially enhanced by the addition of both Mo and Mn compared to Mo alone.

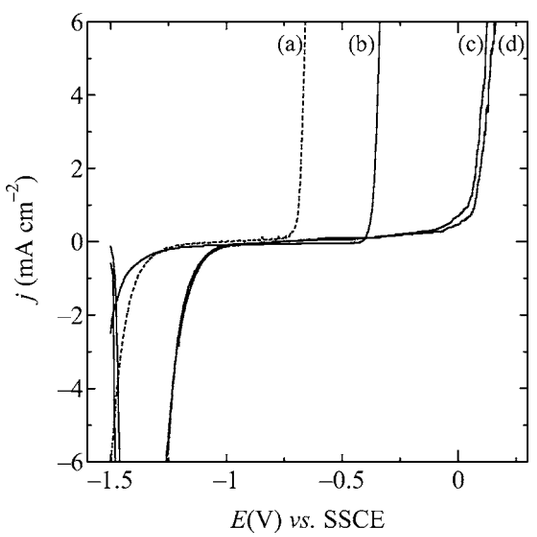

Figure 7. Anodic polarization curves recorded in deaerated 0.1 mol L^{-1} aqueous NaCl for (a) pure Al, (b) $Al_{95.8}Mn_{4.2}$, (c) $Al_{90.8}Mo_{5.5}Mn_{3.7}$, and (d) $Al_{87.9}Mo_{7.6}Mn_{4.5}$. The temperature was ~298 K, and the scan rate was 0.5 mV s^{-1}.

Acknowledgment

This research was supported by the Department of Energy, Office of Biological and Environmental Research.

The University of Mississippi assisted in meeting the publication costs of this article.

References

1. T. Tsuda, C. L. Hussey, G. R. Stafford, and J. E. Bonevich, *J. Electrochem. Soc.*, **150**, C234 (2003).
2. G. R. Stafford, T. Tsuda, and C. L. Hussey, *J. Min. and Metall., B*, **39**, 23 (2003).
3. T. Takenaka and M. Kawakami, *Int. J. Mater. Prod. Technol.*, **2**, 500 (2001).
4. T. Tsuda, C. L. Hussey, G. R. Stafford, and O. Kongstein, *J. Electrochem. Soc.*, **151**, C447 (2004).
5. T. Tsuda, C. L. Hussey, and G. R. Stafford, Abstract 692, The Electrochemical Society Meeting Abstracts, Vol. 2003-2, Orlando, FL, Oct 12, 2003
6. T. Tsuda and C. L. Hussey, *J. Min. and Metall., B*, **39**, 3 (2003).
7. M. Matsunaga, M. Morimitsu, M. Nagano, and T. Tsuda, *Molten Salt Forum*, **5–6**, 601 (1998).
8. M. R. Ali, A. Nishikata, and T. Tsuru, *Electrochim. Acta*, **42**, 2347 (1997).
9. M. Matsunaga, T. Kitazaki, K. Hosokawa, S. Hirano, and M. Yoshida, in *Proceedings of the Ninth International Symposium on Molten Salts*, C. L. Hussey, D. S. Newman, G. Mamantov, and Y. Ito, Editors, PV 94-13, p. 422, The Electrochemical Society Proceedings Series, Pennington, NJ (1994).
10. W. R. Pitner, C. L. Hussey, and G. R. Stafford, *J. Electrochem. Soc.*, **143**, 130 (1996).
11. L. Heerman and W. D'Olieslager, in *Proceedings of the Ninth International Symposium on Molten Salts*, C. L. Hussey, D. S. Newman, G. Mamantov, and Y. Ito, Editors, PV 94-13, p. 441, The Electrochemical Society Proceedings Series, Pennington, NJ (1994).
12. R. J. Gale, B. Gilbert, and R. A. Osteryoung, *Inorg. Chem.*, **18**, 2723 (1979).
13. R. T. Carlin, H. C. De Long, J. Fuller, and P. C. Trulove, *J. Electrochem. Soc.*, **145**, 1598 (1998).
14. M. R. Ali, A. Nishikata, and T. Tsuru, *Electrochim. Acta*, **42**, 1819 (1997).
15. J. A. Mitchell, W. R. Pitner, C. L. Hussey, and G. R. Stafford, *J. Electrochem. Soc.*, **143**, 3448 (1996).
16. R. T. Carlin, P. C. Trulove, and H. C. De Long, *J. Electrochem. Soc.*, **143**, 2747 (1996).
17. Q. Zhu, C. L. Hussey, and G. R. Stafford, *J. Electrochem. Soc.*, **149**, C268 (2002).
18. Q. Zhu and C. L. Hussey, *J. Electrochem. Soc.*, **148**, C395 (2001).
19. G. R. Stafford, V. D. Jovic, and C. L. Hussey, *Mater. Sci. Forum*, **352**, 49 (2000).
20. B. J. Tierney, W. R. Pitner, J. A. Mitchell, C. L. Hussey, and G. R. Stafford, *J. Electrochem. Soc.*, **145**, 3110 (1998).

21. G. R. Stafford and C. L. Hussey, in *Advances in Electrochemical Science and Engineering*, Vol. 7, R. C. Alkire and D. M. Kolb, Editors, p. 275, Wiley-VCH Verlag GmbH, Weinheim, Germany (2002).
22. T. Tsuda, C. L. Hussey, and G. R. Stafford, *J. Electrochem. Soc.*, **151**, C379 (2004).
23. T. P. Moffat, G. R. Stafford, and D. E. Hall, *J. Electrochem. Soc.*, **140**, 2779 (1993).
24. J. Uchida, T. Tsuda, Y. Yamamoto, H. Seto, M. Abe, and A. Shibuya, *ISIJ Int.*, **33**, 1029 (1993).
25. J. Uchida, A. Shibuya, T. Tsuda, Y. Yamamoto, and H. Seto, *The Sumitomo Search*, **44**, 126 (1990).
26. G. R. Stafford, *J. Electrochem. Soc.*, **136**, 635 (1989).
27. J. S. Wilkes, J. A. Levisky, R. A. Wilson, and C. L. Hussey, *Inorg. Chem.*, **21**, 1263 (1982).
28. P. C. Trulove, J. A. Mitchell, P. L. Hagans, R. T. Carlin, G. R. Stafford, and H. C. De Long, in *Twelfth International Symposium on Molten Salts*, P. C. Trulove, H. C. De Long, G. R. Stafford, and S. Deki, Editors, PV 99-41, p. 517, The Electrochemical Society Proceedings Series, Pennington, NJ (2000).
29. L. Qingfeng, H. A. Hjuler, R. W. Berg, and N. J. Bjerrum, *J. Electrochem. Soc.*, **137**, 2794 (1990).